Computers in Biology and Medicine 39 (2009) 412 – 424

Contents lists available at ScienceDirect

Computers in Biology and Medicine

journal homepage: www.elsevier.com/locate/cbm

Mesoscale modeling technique for studying the dynamics oscillation of Min protein: Pattern formation analysis with lattice Boltzmann method

Somchai Sriyab[a,b], Jiraporn Yojina[a,b], Waipot Ngamsaad[b], Paisan Kanthang[b], Charin Modchang[b], Narin Nuttavut[b], Yongwimon Lenbury[a,e], Chartchai Krittanai[c], Wannapong Triampo[b,d,f,*]

[a]Department of Mathematics, Faculty of Science, Mahidol University, Bangkok, Thailand
[b]R&D Group of Biological and Environmental Physics, Department of Physics, Faculty of Science, Mahidol University, Bangkok, Thailand
[c]Center of Excellence for Vector and Vector-Borne Diseases, Faculty of Science, Mahidol University, Nakhonpathom, Thailand
[d]Institute of Molecular Biology and Genetics, Mahidol University, Nakhonpathom, Thailand
[e]Center of Excellence in Mathematics, PERDO, Commission on Higher Education, Thailand
[f]Thailand Center of Excellence in Physics, PERDO, Commission on Higher Education, Thailand

ARTICLE INFO

Article history:
Received 12 May 2008
Accepted 11 February 2009

Keywords:
Lattice Boltzmann method
Protein oscillation
Min proteins
Pattern formation
Mesoscale

ABSTRACT

We presented an application of the Lattice Boltzmann method (LBM) to study the dynamics of Min proteins oscillations in *Escherichia coli*. The oscillations involve MinC, MinD and MinE proteins, which are required for proper placement of the division septum in the middle of a bacterial cell. Here, the LBM is applied to a set of the deterministic reaction diffusion equations which describes the dynamics of the Min proteins. This determines the midcell division plane at the cellular level. We specifically use the LBM to study the dynamic pole-to-pole oscillations of the Min proteins in two dimensions. We observed that Min proteins' pattern formation depends on the cell's shape. The LBM numerical results are in good agreement with previous findings, using other methods and agree qualitatively well with experimental results. Our results indicate that the LBM can be an alternative computational tool for simulating the dynamics of these Min protein systems and possibly for the study of complex biological systems which are described by reaction–diffusion equations. Moreover, these findings suggest that LBM could also be useful for the investigation of possible evolutionary connection between the cell's shape and cell division of *E. coli*. The results show that the oscillatory pattern of Min protein is the most consistent with experimental results when the dimension of the cell is 1×2. This suggests that as the cell's shape is close to being a square, the oscillatory pattern no longer places the cell division of *E. coli* at the proper location. These findings may have a significant implication on why, by natural selection, *E. coli* is maintained in a rod shape or bacillus form.

1. Introduction

Cell division is the process that a cell separates into two daughter cells after the DNA has been duplicated and distributed into two regions. For a successful cell division, the cell has to determine where to separate in *Escherichia coli* and other rod-shape bacteria, two processes are known to determine the division site: nucleoid occlusion [1] and the oscillation of Min proteins [2].

Min proteins which are involved in determining the division site are the MinC, MinD, and MinE proteins [2]. Experiments involving the use of modified proteins have shown that MinC is able to inhibit the formation of the filamentous temperature sensitiveZ (FtsZ)-ring [3]. It has been reported that tubules of FtsZ protein form cytoskeleton structure that is involved in septum formation [46]. The FtsZ moves from the cytoplasm to inner membrane at the midcell location just prior to cell division and assembles the Z-ring which then relocates to the cytoplasm after division. MinD, on the other hand, is an ATPase which is connected peripherally to the cytoplasmic membrane. It can bind and activate MinC into function [4,5]. Recent studies have demonstrated that MinD recruits MinC to the membrane. This suggests that MinD stimulates MinC by concentrating them near the presumed site of activation [6,7]. MinE is required to give site specificity to division inhibitor, which suggests that MinE acts as a topological specificity protein capable of recognizing the midcell site and preventing the MinC division inhibitor from acting at that site [8]. Its expression results in a site-specific suppression

* Corresponding author at: R&D Group of Biological and Environmental Physics, Department of Physics, Faculty of Science, Mahidol University, Rama 6 Rd., Ratchatewee, Bangkok 10400, Thailand. Tel.: +66 2 441 9816x1131; fax: +66 2 441 9322.
E-mail addresses: scwtr@mahidol.ac.th, wtriampo@gmail.com (W. Triampo).

0010-4825/$ - see front matter © 2009 Elsevier Ltd. All rights reserved.
doi:10.1016/j.compbiomed.2009.02.003

of the MinC/MinD action so that the FtsZ assembly is allowed in the middle of the cell, but is inhibited at other sites [2]. In the absence of MinE, the MinC/MinD is distributed homogeneously over the entire membrane. These results in a complete blockage of the Z-ring formation and the subsequent formation of a long filamentous cell which would fail to divide [6,7,9,10]. By a fluorescent labeling technique, MinE was shown to attach to the cell wall only in the presence of MinD [11,12]. Since MinD interacts with MinC, it is likely that they oscillate together. This results in a concentration of the division inhibitor at the membrane on either cell end, alternating between being high or low every 20 seconds, so that the period of oscillation is about 40 s [6,7]. MinE is not only required for the MinC/MinD oscillation, it is also involved in setting the frequency of the oscillation cycle [9]. Several pieces of evidence indicate that the MinE localization cycle is tightly coupled with the oscillation cycle of MinD. Experimentally, microscopy of fluorescently labeled proteins involved in the regulation of *E. coli* division is uncovered coherent and stable spatial and temporal oscillations of these three proteins [13]. The proteins oscillate from one end of the bacterium to the other and move between the cytoplasmic membrane and the cytoplasm. The detailed mechanism by which these proteins determine the accurated position of the division plane is currently unknown, but the observed pole-to-pole oscillations of the corresponding distribution are thought to be of functional importance.

A number of mathematical models of Min protein oscillation have been proposed and studied [11,14–18]. These models are based on macroscopic nonlinear reaction–diffusion equations (RDE) and are solved using conventional finite difference schemes. Howard et al. [14] proposed an RDE model in which the reaction consisted of protein's association to the membrane and its dissociation from the membrane. This model incorporates the event that MinE is recruited to the membrane by membrane-associated MinD. Later, Meinhardt et al. [15] showed that the pattern formation of the Min system requires the interaction of a self-enhancing component and its long-ranging antagonists. They included the dynamics of FtsZ proteins in their model. More recently, Kruse et al. [16] found that the pole-to-pole oscillation depends on a tendency of cytoplasmic membrane MinD to cluster and attachment to and detachment from the cell wall. However, the Kruse model requires unrealistically rapid membrane diffusion of MinD. Since most models mentioned above applied only to uniformly rod-shaped wild-type cells, Huang and Wingreen [18] proposed the model to reproduce the experimental oscillations in not only rod-shaped cells, but also round and ellipsoidal cells. All of these models successfully generated the oscillation patterns and are in agreement with the experimental observations. Huang et al. [11] formulated the model in three dimensions based on an experiment to describe Min proteins oscillation. All these models only deal with the macroscopic behavior, modeled by the RDE and do not provide microscopic details. This present work focused on the reaction of MinD and MinE and presented an alternative method, called the Lattice Boltzmann method (LBM) [19], for determining the position of cell division of *E. coli* which depended on the mechanism of Min system in the microscopic level.

The LBM scheme has been particularly successful in simulating fluid flow and useful for a broad variety of complex physical systems, finding applications in different areas, such as in hydrodynamic systems [19,20], magneto-hydrodynamics [21–24], multiphase and multi-component fluids [25], advection–diffusion [26], reaction–diffusion [27–30] and blood flow [31–33]. Most research reported in the literature is limited to the applications of LBM to the Navier–Stokes equations [34,35]. Its application to complex biological systems at the cellular and the molecular biological levels is rare.

In this work, we propose the use of LBM to study the partitioning of a bacterial cell during cell division and compare our two-dimensional results with experimental observations.

2. Reaction–diffusion models for Min protein oscillation

We consider RDE model consisting of a set of four partial differential equations in order to study the Min protein oscillation. This is a version that is one dimensional in the space variable, given by Howard et al. [14]. Though the model is straightforward and relatively simple, it gives the correct placement of the division septum in *E. coli*. The mechanism is governed by the time rates of change of the protein densities due to the diffusions of MinD and MinE and to the mass transfer between the cell membrane and the cytoplasm as schematically shown in Fig. 1. Based on experimental results [7], showing that the MinC dynamics are similar to those of MinD, we shall leave out the equations for the MinC proteins. In dimensionless form, the dynamics may be given by the following equations:

$$\frac{\partial \rho_D}{\partial t} - D_D \nabla^2 \rho_D = R_D = -\frac{\sigma_1 \rho_D}{1+\sigma_1' \rho_e} + \sigma_2 \rho_e \rho_d, \tag{1}$$

$$\frac{\partial \rho_d}{\partial t} - D_d \nabla^2 \rho_d = R_d = \frac{\sigma_1 \rho_D}{1+\sigma_1' \rho_e} - \sigma_2 \rho_e \rho_d, \tag{2}$$

$$\frac{\partial \rho_E}{\partial t} - D_E \nabla^2 \rho_E = R_E = \frac{\sigma_4 \rho_e}{1+\sigma_4' \rho_D} - \sigma_3 \rho_D \rho_E, \tag{3}$$

$$\frac{\partial \rho_e}{\partial t} - D_e \nabla^2 \rho_e = R_e = -\frac{\sigma_4 \rho_e}{1+\sigma_4' \rho_D} + \sigma_3 \rho_D \rho_E, \tag{4}$$

where ∇^2 is the Laplacian operator. We let $s=\{D,d,E,e\}$ represent the cytoplasmic MinD, the cytoplasmic membrane MinD, the cytoplasm MinE, and the cytoplasmic membrane MinE, respectively. Here, ρ_s is the mass density of particles of species s at time t and position (x,y). R_s is a reaction term which depends on the density of the species (ρ_s) and on the density of the other species that react with species s. D_s is the diffusion coefficient, σ_1 is the parameter connected to the spontaneous association of MinD to the cytoplasmic membrane, σ_1' is that which is connected to suppression of MinD recruitment from the cytoplasm by the membrane-bound MinE, and the σ_2 reflects the rate that MinE on the membrane drives the MinD on the membrane into the cytoplasm. We let σ_3 be the rate that cytoplasmic MinD recruits cytoplasmic MinE to the membrane, while σ_4 describes the rate of dissociation of MinE from the membrane to the cytoplasm. Finally, σ_4' reflects the cytoplasmic MinD suppression of the release of the membrane-bound MinE. The diffusion on the membrane occurs at a much smaller time scale than that in the cytoplasm. It seems, therefore, reasonable to set D_d and D_e as zero. In this dynamics, we allow the Min protein to bind to/unbind from the membrane, but not

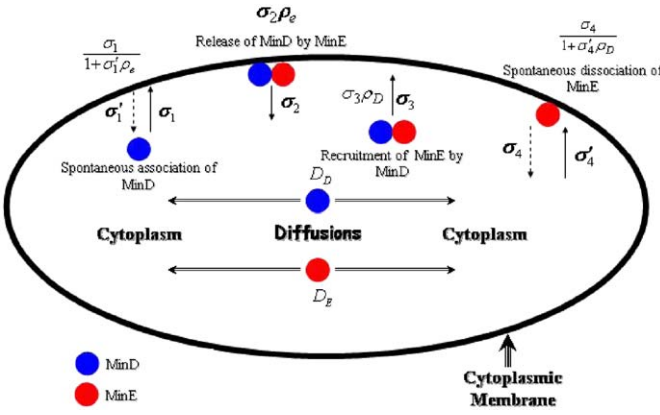

Fig. 1. Schematic diagram of the MinDE dynamics. This model of the mechanisms of MinD and MinE interaction was proposed by Howard et al. [14]. This figure shows the rate reaction of Min proteins in the cytoplasm and cytoplasmic membrane.

for it to be degraded in the process. Thus, the total amount for each type of Min protein is conserved. The zero-flux boundary condition will be imposed. This boundary condition needs a closed system with reflecting or hard-wall boundary conditions. The total concentration of Min proteins is conserved.

Before turning to numerical description of this model, we first analytically work out the linear stability of the model system in one spatial dimension as the following.

2.1. Stability analysis

To determine whether the steady state is stable against small spatial perturbations, linear stability analysis is performed. For simplicity, we write our set of Eqs. (1)–(4) in one-dimensional spatial form

$$\frac{\partial \vec{\rho}}{\partial t} = \mathbf{D}\frac{\partial^2 \vec{\rho}}{\partial x^2} + \vec{f}(\vec{\rho}), \tag{5}$$

where $\vec{\rho}$ is the Min proteins density vector, $\mathbf{D}$ is a diffusion matrix, and $\vec{f}(\vec{\rho})$ is a nonlinear function of $\vec{\rho}$. Suppose $\vec{\rho}^*$ is a homogeneous fixed point of Eq. (5), then we define

$$\vec{\rho} \equiv \delta\vec{\rho} + \vec{\rho}^*, \tag{6}$$

where $\delta\vec{\rho}$ is a small variation from the fixed point. Substituting (6) in (5), we obtain

$$\frac{\partial \delta\vec{\rho}}{\partial t} = \mathbf{D}\frac{\partial^2 \delta\vec{\rho}}{\partial x^2} + \vec{f}(\vec{\rho}^* + \delta\vec{\rho}). \tag{7}$$

Then we take a multivariate Taylor expansion of $\vec{f}(\vec{\rho}^* + \delta\vec{\rho})$ around the homogeneous fixed point $\vec{\rho}^*$

$$\begin{aligned}\vec{f}(\vec{\rho}^* + \delta\vec{\rho}) &= \vec{f}(\vec{\rho}^*) + \left.\frac{\partial \vec{f}}{\partial \vec{\rho}}\right|_{\vec{\rho}^*} \delta\vec{\rho} + \dots \\ &= \left.\frac{\partial \vec{f}}{\partial \vec{\rho}}\right|_{\vec{\rho}^*} \delta\vec{\rho} + \dots \\ &= \mathbf{J}^*\delta\vec{\rho} + \dots,\end{aligned} \tag{8}$$

where $\mathbf{J}^*$ is the Jacobian matrix evaluated at the fixed point $\vec{\rho}^*$ and the Jacobian matrix is defined as

$$\mathbf{J} = \begin{bmatrix} \frac{\partial f_1}{\partial \rho_1} & \frac{\partial f_1}{\partial \rho_2} & \cdots & \frac{\partial f_1}{\partial \rho_n} \\ \frac{\partial f_2}{\partial \rho_1} & \frac{\partial f_2}{\partial \rho_2} & \cdots & \frac{\partial f_2}{\partial \rho_n} \\ \vdots & \vdots & & \vdots \\ \frac{\partial f_n}{\partial \rho_1} & \frac{\partial f_n}{\partial \rho_2} & \cdots & \frac{\partial f_n}{\partial \rho_n} \end{bmatrix}.$$

For a small variation from the fixed point, only the first term in Eq. (8) is significant. If we want to know how trajectories behave near the equilibrium point, e.g. whether they move toward or away from the equilibrium point, it should therefore be good enough to keep just this term. Then we have

$$\vec{f}(\vec{\rho}^* + \delta\vec{\rho}) = \mathbf{J}^*\delta\vec{\rho}. \tag{9}$$

Substituting (9) in (7), we obtain

$$\frac{\partial \delta\vec{\rho}}{\partial t} = \mathbf{D}\frac{\partial^2 \delta\vec{\rho}}{\partial x^2} + \mathbf{J}^*\delta\vec{\rho}. \tag{10}$$

Since the matrix $\mathbf{J}^*$ is a constant matrix, this is just a set of linear differential equations. Now, suppose the solution has the form

$$\delta\vec{\rho} = \delta\vec{\rho}_0 e^{\omega t} e^{iqx}. \tag{11}$$

Substituting (11) in (10), we have

$$\omega\delta\vec{\rho} = -\mathbf{D}q^2\delta\vec{\rho} + \mathbf{J}^*\delta\vec{\rho}.$$

So, ω is just the eigenvalues of the equation

$$(-\mathbf{D}q^2 + \mathbf{J}^*)\delta\vec{\rho} = \omega\delta\vec{\rho}. \tag{12}$$

The real part of ω will determine whether the equations are linearly stable under a small spatial perturbation, whereas its imaginary part will determine the period of the oscillation

$$T = \frac{2\pi}{|\mathrm{Im}(\omega)|}. \tag{13}$$

If we know that there exists only one eigenvalue ω whose real part is positive, then we can conclude that this homogeneous fixed point is linearly unstable under a small spatial perturbation. We use an iterative method to find the homogeneous fixed point of our set of Eqs. (1)–(4). We carried out the iterations several times with different starting points, using parameter values given by Howard et al. [14], finding only one fixed point, namely $\rho_D = 747.06$, $\rho_E = 0.00$, $\rho_d = 2.94$, $\rho_e = 750.00$. With this fixed point together with Eq. (12), we are able to find the eigenvalues ω and determine if, for a certain set of parameter values, the fixed point is linearly stable. Now, we turn to application of LBM and numerical results.

3. The Lattice Boltzmann Method

The LBM is a numerical scheme evolved from the Lattice gas model (LGM) in order to overcome the difficulties encountered with that model [19,36]. The LGM or lattice gas automata is a method to determine the kinetics of particles by utilizing a discrete lattice and discrete time. It has provided insights into the underlying microscopic dynamics of the physical system whereas most other approaches focus only on the solution to the macroscopic equation. However, the LGM, in which the particles obey an exclusion principle, has microscopic collision rules. These rules are very complicated and require many random numbers. These random numbers create noise or fluctuations. An ensemble averaging is then required to smooth out the noise in order to obtain the macroscopic dynamics which are the results of the collective behavior of the many microscopic particles in the system and which are not sensitive to the underlying details at the microscopic level. The ensemble averaging consumes computer resources, which leads to an increase in the amount of computational storage required and which in turn leads to a reduction in the computational speed. For these reasons, the LBM is used only when one is interested in the evolution of averaged quantities and not in the influence of the fluctuations. The LBM gives a correct average description on the macroscopic level of a fluid. Though LBM is based on particle dynamics, its central focus is the averaged macroscopic behavior, leaving out the fluctuation. It is relatively easy to implement the more complex boundary condition such as the curved boundary [37] when compared with the conventional grid-based numerical integration. In addition, for the model whose dynamics is very complex, use of parallel computing [19] in combination with LBM algorithm would be greatly beneficial in terms of simulating time in a straight forward manner.

The LBM can also be viewed as a special finite difference scheme for the kinetic equation of the discrete-velocity distribution

function. While the traditional computational methods in fluid dynamics, such as finite element method, finite difference method and finite volume method, solve macroscopic fluid dynamics equations, LBM solves a problem at a microscopic level in order to recover a particle density and velocity from the macroscopic properties [38]. The simplicity and the kinetic nature of the LBM are among its appealing features. The LBM consists of simple arithmetic calculations and is, therefore, easy to program. In the LBM, the space is divided into a regular Cartesian lattice grid as a consequence of the symmetry of the discrete-velocity set. Each lattice point has an assigned set of velocity vectors with specified magnitudes and directions connecting the lattice point to its neighboring lattice points. The total velocity and particle density are defined by specifying the number of particles associated with each of the velocity vectors. The microscopic particle distribution function, which is the only unknown, evolves at each time step through a two-step procedure: convection and collision. The first step, convection (or streaming), simply advances the particles from one lattice site to another lattice site along the directions of motion according to their velocities. This feature is borrowed from the kinetic theory. The second step, or collision, is to imitate various interactions among particles by allowing for the relaxation of a distribution do toward an equilibrium distribution through a linear relaxation parameter. The averaging process uses information based on the whole velocity phase space.

The lattice Boltzmann equation can be viewed as a discrete form of the Boltzmann equation. LBM can be derived directly from the simplified Boltzmann Bhatnagar–Gross–Krook (BGK) equation [39,40]. The discrete form of the lattice Boltzmann equation is

$$f_\alpha(\vec{r}+\Delta t\vec{c}_\alpha, t+\Delta t) = f_\alpha(\vec{r},t) + \Omega_\alpha(\vec{r},t), \tag{14}$$

where f_α is the distribution function at space $\vec{r}$ and time t. With the discrete velocity $\vec{c}_\alpha$, the particle distribution travels to the next lattice node in one time step Δt. The collision operator Ω_α differs according to the model details. In the lattice BGK (LBGK) that we use, the particle distribution after propagation is relaxed toward the equilibrium distribution $f_i^{eq}(\vec{r},t)$ according to

$$\Omega_\alpha(\vec{r},t) = -\frac{1}{\tau}(f_\alpha(\vec{r},t) - f_\alpha^{eq}(\vec{r},t)). \tag{15}$$

The relaxation parameter τ determines the kinematic viscosity υ of the simulated flow according to

$$\upsilon = (2\tau - 1)/6.$$

LBM, as the name suggests, works on the given lattice depending on the field of applications. Traditionally, the interested systems are named DXQY, where X is the number of dimensions and Y determines the number of distinct lattice velocities.

The equilibrium distribution function f^{eq} is defined to be the same for one, two, and three dimensions as

$$f_\alpha^{eq} = \omega_\alpha \rho\left(1 + \frac{3c_\alpha\cdot\vec{u}}{c^2} + \frac{9(c_\alpha\cdot\vec{u})^2}{2c^4} - \frac{3u^2}{2c^2}\right), \tag{16}$$

where the weight constant and the lattice velocities for D1Q3 are

$$\omega_\alpha = \begin{cases} 2/3, & \alpha = 0 \\ 1/6, & \alpha = 1,2 \end{cases}, \tag{17}$$

$$c_\alpha = \begin{cases} 0, & \alpha = 0 \\ \cos(\alpha-1), & \alpha = 1,2 \end{cases} \tag{18}$$

while the weight constant and the lattice velocities for D2Q9 are

$$\omega_\alpha = \begin{cases} 4/9 & \alpha = 0 \\ 1/9, & \alpha = 1,2,3,4 \\ 1/36, & \alpha = 5,6,7,8 \end{cases}, \tag{19}$$

$$c_\alpha = \begin{cases} (0,0), & \alpha = 0 \\ c(\cos\theta_\alpha, \sin\theta_\alpha), & \theta_\alpha = (\alpha-1)\pi/2, \ \alpha = 1,2,3,4 \\ \sqrt{2}c(\cos\theta_\alpha, \sin\theta_\alpha), & \theta_\alpha = (\alpha-5)\pi/2 + \pi/4, \ \alpha = 1,2 \end{cases}, \tag{20}$$

and the weight constant and lattice velocities for D3Q27 are

$$\omega_\alpha = \begin{cases} 8/27, & \alpha = 0 \\ 2/27, & \alpha = 1,2,\ldots,6 \\ 1/54, & \alpha = 7,8,\ldots,18 \\ 1/216, & \alpha = 19,20,\ldots,26 \end{cases}, \tag{21}$$

$$c_\alpha = \begin{cases} (0,0,0), & \alpha = 0 \\ c(\pm1,0,0), c(0,\pm1,0), & \\ \quad c(0,0\pm1), & \alpha = 1,2,\ldots,6 \\ c(\pm1,\pm1,0), c(\pm1,0,\pm1), & \\ \quad c(0,\pm1,\pm1), & \alpha = 7,8,\ldots,18 \\ c(\pm1,\pm1,\pm1), & \alpha = 19,20,\ldots,26 \end{cases}. \tag{22}$$

The density ρ and flow velocity u can be calculated from

$$\rho = \sum_\alpha f_\alpha, \tag{23}$$

$$\rho u = \sum_\alpha c_\alpha f_\alpha. \tag{24}$$

For simplicity, the size of a cell and the length of time step will be normalized to 1, which leads to $c=1$, and will not be included in the formulas. We summarize LBM as

$$f_\alpha(\vec{r}+\vec{c}_\alpha, t+1) - f_\alpha(\vec{r},t) = -\frac{1}{\tau}(f_\alpha - f_\alpha^{eq}). \tag{25}$$

Due to the fact that the Navier–Stokes equations are the continuum limit of the lattice Boltzmann, they can be derived by a procedure called Chapman–Enskog expansion, or multiscale analysis. To do so we must first Taylor expand LBM Eq. (25). We then have

$$\begin{aligned} &f_\alpha(\vec{r}+\vec{c}_\alpha, t+1) - f_\alpha(\vec{r},t) \\ &\quad\approx \left(\frac{\partial}{\partial t} + \vec{c}_\alpha\cdot\nabla\right) f_\alpha(\vec{r},t) + \frac{1}{2}\left(\frac{\partial}{\partial t} + \vec{c}_\alpha\cdot\nabla\right)^2 f_\alpha(\vec{r},t) + O(\varepsilon^2) \\ &\quad= -\frac{1}{\tau}(f_\alpha - f_\alpha^{eq}). \end{aligned} \tag{26}$$

Expanding the distribution function and the time and space derivatives in term of the Knudsen number ε, one obtains

$$f_\alpha = f_\alpha^{(0)} + \varepsilon f_\alpha^{(1)} + \varepsilon^2 f_\alpha^{(2)} + O(\varepsilon^3), \tag{27}$$

$$\frac{\partial}{\partial t} = \varepsilon\frac{\partial}{\partial t_1} + \varepsilon^2\frac{\partial}{\partial t_2}, \tag{28}$$

$$\nabla = \varepsilon\nabla_1, \tag{29}$$

where $f^{(0)} = f^{eq}$. The above formula assumes that the diffusion time scale t_2 is much smaller than convection time scale t_1. Eqs. (27)–(29) satisfy the constraints

$$\sum_\alpha f_\alpha^{(0)} = \rho, \tag{30}$$

$$\sum_\alpha e_\alpha f_\alpha^{(0)} = \rho u, \tag{31}$$

when

$$\sum_{\alpha} f_{\alpha}^{(k)} = 0, \tag{32}$$

$$\sum_{\alpha} e_{\alpha} f_{\alpha}^{(k)} = 0. \tag{33}$$

For $k > 0$. Substituting Eqs. (27)–(29) into Eq. (26), we have

$$\left(\varepsilon\frac{\partial}{\partial t_1} + \varepsilon^2\frac{\partial}{\partial t_2} + \varepsilon\vec{c}_{\alpha}\cdot\nabla_1\right)(f_{\alpha}^{(0)} + \varepsilon f_{\alpha}^{(1)} + \varepsilon^2 f_{\alpha}^{(2)}) + \left(\varepsilon\frac{\partial}{\partial t_1} + \varepsilon^2\frac{\partial}{\partial t_2} + \varepsilon\vec{c}_{\alpha}\cdot\nabla_1\right)^2(f_{\alpha}^{(0)} + \varepsilon f_{\alpha}^{(1)} + \varepsilon^2 f_{\alpha}^{(2)}) = -\frac{1}{\tau}(\varepsilon f_{\alpha}^{(1)} + \varepsilon^2 f_{\alpha}^{(2)}). \tag{34}$$

We obtain the following equation from terms of order ε:

$$\left(\frac{\partial}{\partial t_1} + \vec{c}_{\alpha}\cdot\nabla_1\right) f_{\alpha}^{(0)} = -\frac{1}{\tau} f_{\alpha}^{(1)}, \tag{35}$$

and terms of order ε^2 yield

$$\frac{\partial f_{\alpha}^{(0)}}{\partial t_2} + \left(\frac{\partial}{\partial t_1} + \vec{c}_{\alpha}\cdot\nabla_1\right) f_{\alpha}^{(1)} + \frac{1}{2}\left(\frac{\partial}{\partial t_1} + \vec{c}_{\alpha}\cdot\nabla_1\right)^2 f_{\alpha}^{(0)} = -\frac{1}{\tau} f_{\alpha}^{(2)}. \tag{36}$$

By using Eq. (35), we can write Eq. (36) as

$$\frac{\partial f_{\alpha}^{(0)}}{\partial t_2} + \left(1 - \frac{1}{2\tau}\right)\left(\frac{\partial}{\partial t_1} + \vec{c}_{\alpha}\cdot\nabla_1\right) f_{\alpha}^{(1)} = -\frac{1}{\tau} f_{\alpha}^{(2)}. \tag{37}$$

Combining (35) with (37), we are led to

$$\frac{\partial}{\partial t_1}\sum_{\alpha} f_{\alpha}^{(0)} + \nabla_1\cdot\sum_{\alpha} c_{\alpha} f_{\alpha}^{(0)} = O(\varepsilon). \tag{38}$$

Continuity is assumed by

$$\frac{\partial \rho}{\partial t} + \nabla\cdot\rho\vec{u} = 0. \tag{39}$$

Using (38) in (39), we have

$$\frac{\partial}{\partial t_1}\sum_{\alpha} c_{\alpha} f_{\alpha}^{(0)} + \nabla_1\cdot\sum_{\alpha} c_{\alpha} c_{\alpha} f_{\alpha}^{(0)} + \varepsilon\left(1 - \frac{1}{2\tau}\right)\nabla_1 \times \sum_{\alpha} c_{\alpha} c_{\alpha} f_{\alpha}^{(1)} = O(\varepsilon). \tag{40}$$

The quantity

$$\sum_{\alpha} c_{\alpha} c_{\alpha} f_{\alpha}^{(0)} = pI + \rho\vec{u}\vec{u} \tag{41}$$

is the stress tensor, where I is the identity tensor. Using Eq. (35) for the term $\varepsilon(1 - 1/2\tau)\nabla_1\cdot\sum_{\alpha} c_{\alpha} c_{\alpha} f_{\alpha}^{(1)}$ in (40) and rearranging, we have

$$-\varepsilon\left(1 - \frac{1}{2\tau}\right)\nabla_1\cdot\sum_{\alpha} c_{\alpha} c_{\alpha}\left(\frac{\partial f_{\alpha}^{(0)}}{\partial t_1} + \nabla_1\cdot\vec{c}_{\alpha} f_{\alpha}^{(0)}\right) = -\upsilon(\nabla_{\alpha}\rho\vec{u}_{\beta} + \nabla_{\beta}\rho\vec{u}_{\alpha}). \tag{42}$$

Lastly, substituting Eqs. (41) and (42) into Eq. (40), we obtain the Navier–Stokes equation

$$\frac{\partial\rho\vec{u}}{\partial t} + \nabla\cdot\rho\vec{u}\vec{u} = -\nabla p + \upsilon\nabla_{\alpha}(\nabla_{\alpha}\rho\vec{u}_{\beta} + \nabla_{\beta}\rho\vec{u}_{\alpha}). \tag{43}$$

The pressure can be calculated from $p = \rho c_s^2$ with speed of sound $c_s = \sqrt{RT}$. The above derivation illustrates how to relate mesoscopic and macroscopic levels of dynamics.

Next, to connect the lattice Boltzmann equation with a reacting system like what we are interested in as shown in Eqs. (1)–(4), we employ a procedure called the Chapmann–Enskog expansion [8]. We then expand the distribution function about the equilibrium as

$$f_{\alpha}^{s} = f_{\alpha}^{s,(0)} + \varepsilon f_{\alpha}^{s,(1)}. \tag{44}$$

We now assume that

$$\frac{\partial}{\partial t} = \varepsilon^2\frac{\partial}{\partial t_2}, \tag{45}$$

$$\nabla = \varepsilon\nabla_1, \tag{46}$$

$$\phi_{\alpha}^{s} = \varepsilon^2\phi_{\alpha}^{s,(2)}. \tag{47}$$

Substituting Eqs. (44)–(47) into Eq. (30), we obtain

$$\vec{c}_{\alpha}\cdot\nabla_1 f_{\alpha}^{s,(0)} = -\frac{1}{\tau_s} f_{\alpha}^{s,(1)} \tag{48}$$

to order ε^1 and

$$\frac{\partial f_{\alpha}^{s,(0)}}{\partial t_2} + \vec{c}_{\alpha}\cdot\nabla_1 f_{\alpha}^{s,(1)} + \frac{1}{2} c_{\alpha} c_{\alpha} : \nabla_1\nabla_1 f_{\alpha}^{s,(0)} = \omega_{\alpha}^{s} R_s \tag{49}$$

to order ε^2. From Eq. (51), we immediately obtain

$$f_{\alpha}^{s,(1)} = -\tau_s\vec{c}_{\alpha}\cdot\nabla_1 f_{\alpha}^{s,(0)}. \tag{50}$$

Inserting Eq. (52) into (51), we have

$$\frac{\partial f_{\alpha}^{s,(0)}}{\partial t_2} + \left(\tau_s - \frac{1}{2}\right) c_{\alpha} c_{\alpha} : \nabla_1\nabla_1 f_{\alpha}^{s,(0)} = \omega_{\alpha}^{s} R_s. \tag{51}$$

Summing Eq. (53) over α, with weights ω_{α}^{s}, we obtain

$$\frac{\partial\rho_s}{\partial t} - \frac{1}{3}\left(\tau_s - \frac{1}{2}\right)\nabla^2\rho_s = R_s, \tag{52}$$

which is the dimensionless version of the initial RDE, in which the relation between the diffusion coefficient and relaxation time is

$$D_s = \tfrac{1}{3}(\tau_s - \tfrac{1}{2}). \tag{53}$$

We consider the two-dimensional LBM (D2Q9) for the RDE in the referenced model. Let $f_{\alpha}^{s}(\vec{r}, t)$ be the one particle distribution function of species s with velocity $\vec{c}_{\alpha}$ at some dimensionless time t and dimensionless space $\vec{r}$.$s = \{1, 2, 3, 4\}$ represent the cytoplasmic MinD, membrane-bound MinD, cytoplasmic MinE and membrane-bound MinE, respectively. The Lattice Boltzmann equation for $f_{\alpha}^{s}(\vec{r}, t)$ can be written as

$$f_{\alpha}^{s}(\vec{r} + \Delta t\vec{c}_{\alpha}, t + \Delta t) = f_{\alpha}^{s}(\vec{r}, t) + \Omega_{\alpha}^{s}(\vec{r}, t), \tag{54}$$

where Ω_{α}^{s} is the collision operator for species s and depends on the distribution function f_{α}^{s}. The collision operator Ω_{α}^{s} can be separated into two parts [27]. The first term is the elastic collision function, which is taken to be of BGK approximation with a single relaxation time τ_s. The second term is reactive collision term, i.e.,

$$\Omega_{\alpha}^{s}(\vec{r}, t) = -\frac{1}{\tau}(f_{\alpha}^{s}(\vec{r}, t) - f_{\alpha}^{(eq,s)}(\vec{r}, t)) + \phi_{\alpha}^{s}, \tag{55}$$

where $f_{\alpha}^{(eq,s)}$ is the equilibrium distribution. Here, we use the simple equilibrium distribution function corresponding to a system with

zero mean flow

$$f_\alpha^{(eq,s)} = \omega_\alpha^s \rho_s, \tag{56}$$

where ω_α^s is the weight function which depends on the lattice symmetry [21].

The density of particle species s is denoted by ρ_s. For the reactive term ϕ_s, we use the simple isotropic form

$$\phi_s = \omega_\alpha^s R_s. \tag{57}$$

The term R_s is the non-linear reaction term and depends on the density of reacting species.

4. LBM numerical implementation

The LBM models flow of particles as an incompressible fluid where particles can move only in the direction of the lattice velocity vectors c_α in a cell. For the simulation, every cell must store the changes in particles that move in the direction of each possible lattice vector c_α, with particle distribution functions f_α, where the values for α are the numbers of the lattice vectors in the cell. The vector c_0 denotes a particle at rest which has zero length.

From the particle distribution functions, two important physical quantities can be calculated. By summing up all distribution functions, we get the density ρ. Another important quantity needed for each cell is the speed and overall direction in which the particle of one cell moves. For this, the momentum density needs to be calculated. It is again the sum of all particle distribution functions, but each distribution function is multiplied first by the lattice vector c_α. The simulation process consists of two steps that are repeated in each time step. To summarize, we will now implement the numerical evaluation governed two equations

$$\text{Collision: } f_\alpha^{s,*}(\vec{r},t) = f_\alpha^s(\vec{r},t) - \frac{1}{\tau}(f_\alpha^s(\vec{r},t) - f_\alpha^{(eq,s)}(\vec{r},t)) + \omega_\alpha^s R_s.$$

$$\text{Streaming: } f_\alpha^s(\vec{r}+\vec{c}_\alpha,t) = f_\alpha^{s,*}(\vec{r},t).$$

The first step is the collision step which accounts for the collision changes due to the movement of particles. The second step is the streaming step, in which the actual movement of the particles takes place throughout the grid. The collision step only changes the distribution of the particles for all particle distribution functions. The most time consuming step is the calculation of $f_\alpha^{(eq)}$ for which we need to calculate the density ρ and velocity $\vec{u}$ first. The streaming step consists only of copying the distribution function f_α from position r to the neighboring $r + c_\alpha$, as shown in Fig. 2. For each cell, all distribution functions are copied to the adjacent cell in the direction of the lattice vector c_α. Hence, for the cell with the coordinates $[i,j]$ the distribution function for the lattice vector pointing upwards is copied to the upward distribution function of cell $[i,j+1]$. As the lattice vector c_0 does not point anywhere, its particle distribution function is not changed in the streaming step. The only trick is, when writing a program that performs the streaming, for each direction c_α, there should be a do loop to copy the distribution function f_α in the opposite direction to that of c_α. This is necessary to prevent any overwriting of distribution functions that are needed for the streaming of another cell.

The boundary treatment is an important issue in the LBM simulations and research advancements are still being made [41,42]. The simplest boundary condition for LBM simulations is the bounce-back scheme, i.e., close to the boundary the fluid does not move at all. Hence, each Lattice Boltzmann cell next to a boundary should have the same amount of particles moving into the boundary as moving into the opposite direction. This will result in a zero velocity, and can be imagined as reflecting the particle distribution functions at the boundary. The reflection process is shown in Fig. 3, for which only the velocities normal to the boundary are reflected. For the implementation this means that boundary and fluid cells need to be distinguished. A flag array has to be introduced and initialized to declare all boundary cells as “wall” and all inner cells as “fluid”. Here the flag array had to be checked, and if the neighboring cell is a boundary cell the opposite distribution function from the current cell would

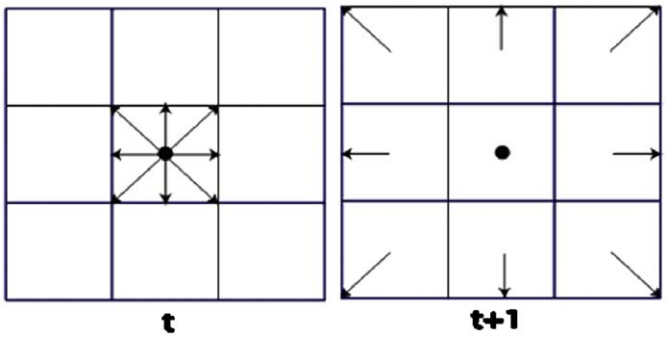

Fig. 2. Particle distribution function in the collision step at time t and the streaming step at time $t+1$ in D2Q9.

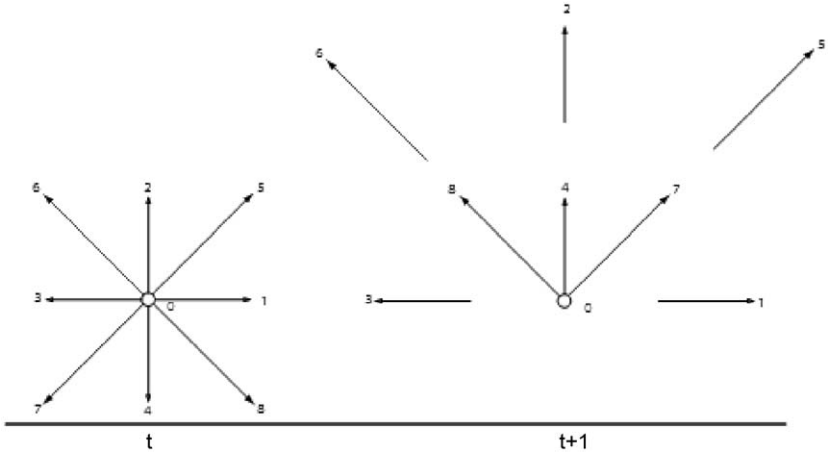

Fig. 3. Sketch of bounce-back scheme.

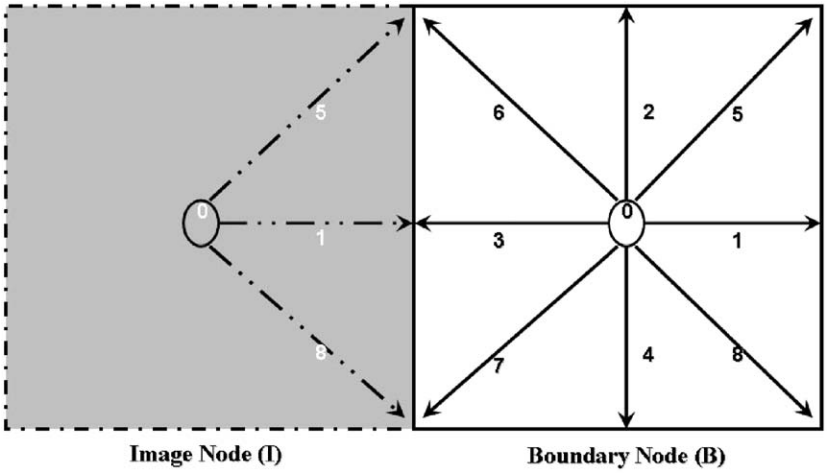

Fig. 4. Schematic illustration of the mirror-image method for the boundary treatment.

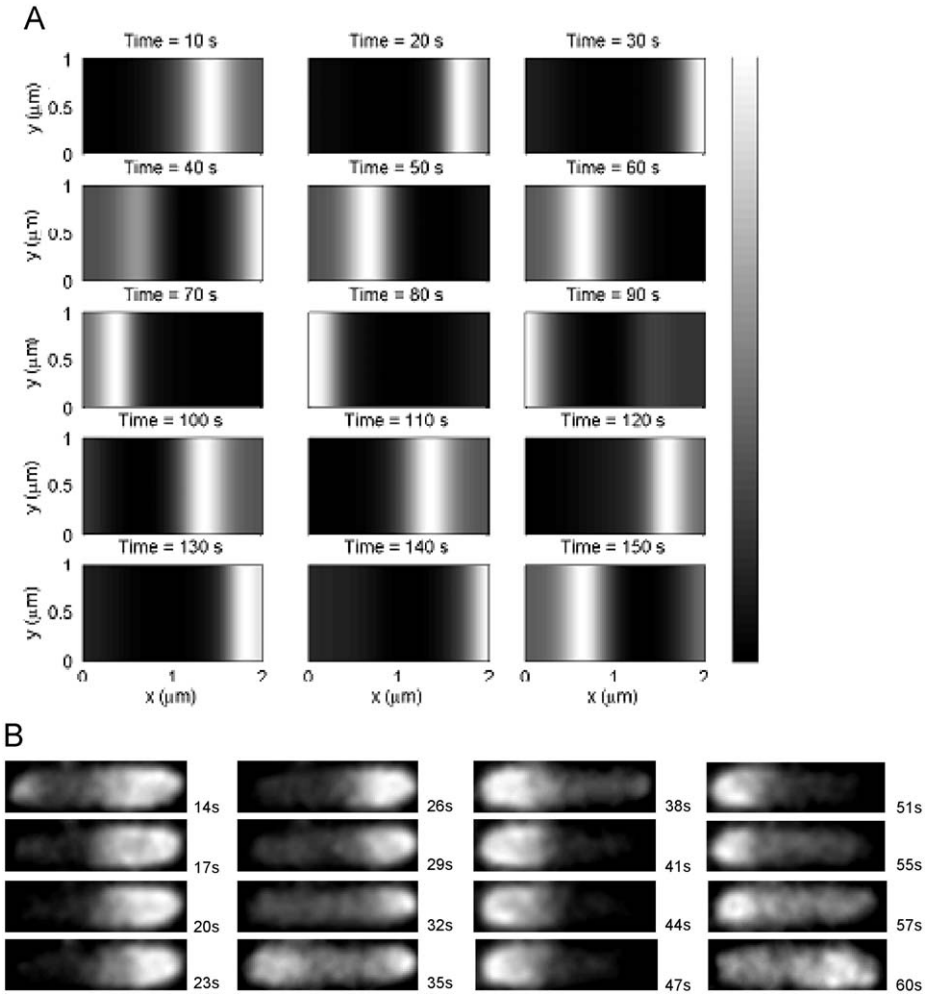

Fig. 5. The oscillation of MinD protein performed in LBM and experiment. (A) The LBM simulation results of MinD showing pole-to-pole oscillation in term of time evolution of total concentration of MinD as a function of position (x,y) (in μm). The color scale runs from the lowest (black) to the highest (white). (B) The experimental results showing the oscillation of GFP:MinD concentration. The characteristics of dynamical pattern are similar features of A and B with MinD mostly concentrated at the polar zone (see experimental details in Ref. [47]).

be taken. The bounce-back scheme is widely used in the treatment of the hard-wall boundary condition. However, we found that the boundary condition is not accurate for the diffusion system. To deal with this, we use the mirror-image method suggested by Zhang et al. [43]. As shown in Fig. 4, if the node *B* is a boundary node, it will see their image in node *I*. The distribution functions are also defined

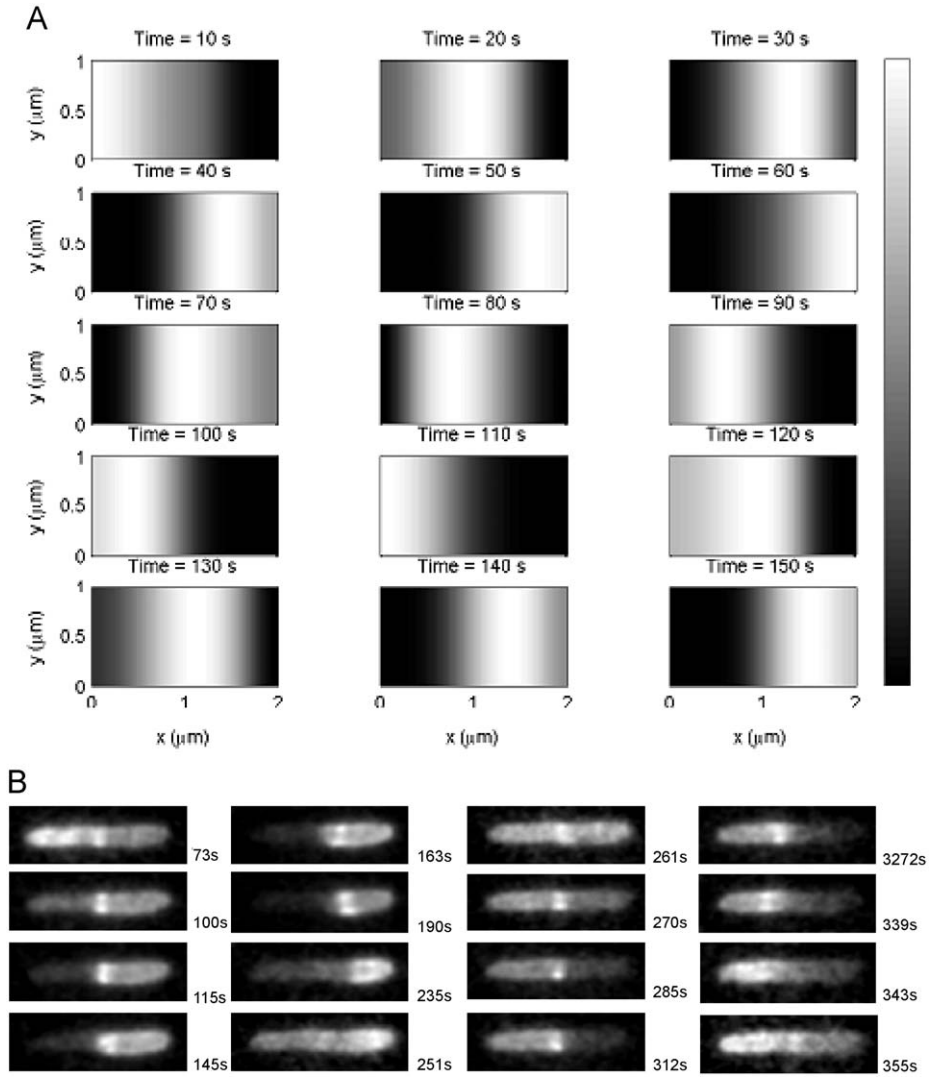

Fig. 6. The oscillation of MinE protein performed in LBM and experiment. (A) The LBM simulation results of MinE showing pole-to-pole oscillation in terms of time evolution of total concentration of MinE as a function of position (x, y) (in μm). The color scale runs from the lowest (black) to the highest (white). (B) The experimental results showing the oscillation of GFP:MinE concentration. The characteristics of dynamical pattern are similar features of A and B while MinE seems to occupy regions near the midcell (see experimental details in Ref. [44]).

at the image node, which serves as the missing distribution function to the real node. The exact form of the distribution functions at the image cell depends on the specific boundary. Here, we use the impermeable boundary which is appropriate for the reaction–diffusion. When the boundary is impermeable, the distribution functions at the imaginary node take the mirrored distribution functions at their real corresponding node. For the example shown in Fig. 4, the pro-collision and pre-streaming distribution functions at the imaginary node I are

$$f_1(I,t) = f_3(B,t),$$
$$f_5(I,t) = f_6(B,t),$$
$$f_8(I,t) = f_7(B,t).$$

This boundary condition is suitable for low speed such as diffusion system, while the bounce-back boundary condition is suitable for high speed flows such as in hydrodynamic systems.

We implemented the LBM, given in Section 3, on a PC using C programming to simulate the two-dimensional model. In the simulation, we use the same parameters as those given by Howard et al. [14], namely

$$D_D = 0.28\,\mu\text{m}^2/\text{s}, \quad D_E = 0.6\,\mu\text{m}^2/\text{s}, \quad D_d = D_e = 0\,\mu\text{m}^2/\text{s},$$
$$\sigma_1 = 20\,\text{s}^{-1}, \quad \sigma_1' = 0.028\,\mu\text{m},$$
$$\sigma_1 = 0.0063\,\mu\text{m/s}, \quad \sigma_2 = 0.04\,\mu\text{m/s},$$
$$\sigma_4 = 0.8\,\text{s}^{-1}, \quad \sigma_4' = 0.8\,\mu\text{m}.$$

However, the LBM algorithm needs all parameters to be dimensionless. We therefore transform the original parameters by letting

$$n = \rho/\rho_0, \quad \tilde{D}_D = D_D\delta t/\delta r^2, \quad \tilde{D}_E = D_E\delta t/\delta r^2, \quad \tilde{\sigma}_1 = \sigma_1\delta t,$$
$$\tilde{\sigma}_1' = \sigma_1'\rho_0, \quad \tilde{\sigma}_2 = \sigma_2\rho_0\delta t,$$
$$\tilde{\sigma}_3 = \sigma_3\rho_0\delta t, \quad \tilde{\sigma}_4 = \sigma_4\delta t, \quad \tilde{\sigma}_4' = \sigma_4'\rho_0,$$

where δt, δr and ρ_0 are, respectively, the time step, grid spacing, and the unit of concentration. Here, we set $\rho_0 = 1/\mu\text{m}$. The relaxation time τ_s is calculated by Eq. (53). The initial numbers of MinD and

MinE are randomly initialized as 3000 for ρ_D, 170 for ρ_E and 0 for ρ_d and ρ_e. Each simulation goes through iterations for 10,000 seconds of time steps. To eliminate transient behavior we throw away the first 10 s into the iterations. We allow the proteins to diffuse in the directions of x- and y-axes and assume that the diffusion is isotropic. For the case of a two-dimensional cell division, we used 50×100 grids to simulate the bacterium (unless otherwise stated), being $1\times2\,\mu m$ in size. The LMB scheme is D2Q9. We choose discrete space steps $\delta_x=\delta_y=2\times10^{-2}\,\mu m$ and time step $\delta t=4\times10^{-4}$ s. We set $\rho_0=1/\mu m^2$ as the concentration unit.

5. Results and discussion

In two dimensions, we plot the time evolution for the concentration of oscillating MinD as shown in Fig. 5, and that of MinE as shown in Fig. 6. The concentrations of Min proteins are homogeneous in the y-axis. The two proteins predominantly oscillate in the x-axis. We compared our computational results, Figs. 5(A) and 6(A), with the experimental results of Unai et al. [47] and Junthorn et al. [44] and found they are in qualitative agreement. It is evident from both numerical and experimental data that MinDs appear near the polar zone as its intensity grows. After that, the intensity decreases, leading to an increase at the opposite pole. It should be emphasized that MinD localizes at the polar zone for relatively longer time and suddenly switches to the opposite pole. Therefore, high concentrations of MinD are mostly found in the polar region. As for the distribution pattern of MinE, the formation is very consistent with experimental data reported in [45], namely it collectively diffuses from the vicinity of midcell to the left edge around the polar zone and immediately returns to the midcell area. Fig. 7 shows time averages of MinD and MinE concentrations. The average concentration of MinD is minimum while that of MinE is maximum at midcell. These patterns once again agree well with the experimental results.

Next, we study the models via LBM to investigate the relationship between a bacterial shape and the distribution patterns of Min proteins. The goal is to understand whether Min proteins dynamics is related to or determine the shape of *E. coli*, and if so how it is. The numerical data might be able to explain why *E. coli* is rod shaped. Hence, we simulated the Min protein oscillation for bacterial cells of several shapes, gradually deviating from an elongated shape and becoming closer to being a square, as shown in Figs. 8–10. Compared to the pattern seen in Fig. 7, the dynamic patterns shown in Figs. 8 and 9, with cell dimensions 2×3 and 3×4, respectively, appear to indicate that the intensity of MinD is maximum away from the poles, while that of MinE is maximum away from the midcell area. When the shape of the cell becomes square, both Min proteins seem to diffuse all over the cell and are not confined to the poles or the midcell (see also Figs. 11–12). In Figs. 8,9, it is clearly seen that the time-average concentrations of MinD (MinE) are no longer predicted by the model to be lowest (highest) at the center of the length of

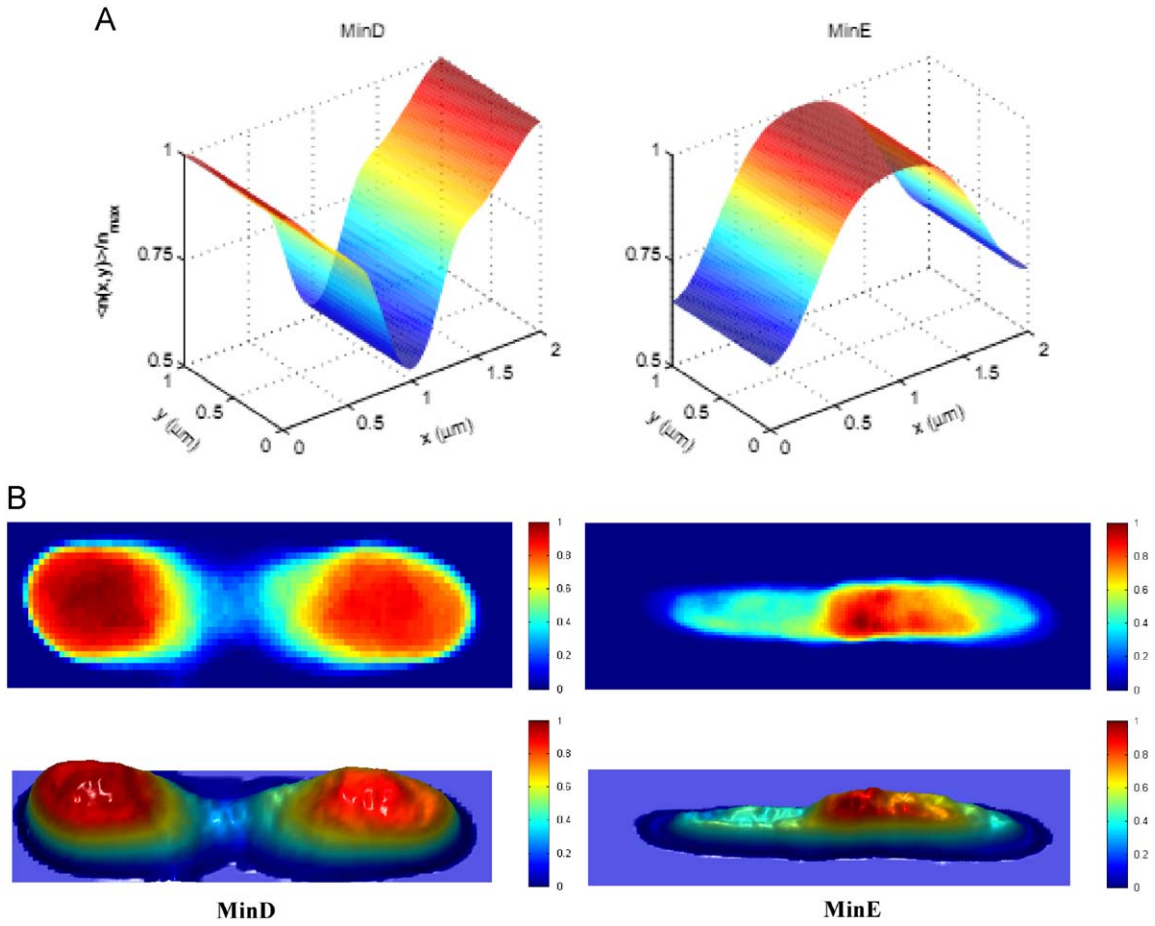

Fig. 7. The time average of MinD and MinE by LBM and experiment. (A) The time average MinD (left) and MinE (right) densities $\langle n(x,y)\rangle/n_{max}$ in LBM simulation, relative to their respective time-average maxima, as a function of two-dimensional position $\vec{x}=(x,y)$ (in μm) along the bacterium. The bacterial shape is $1\times2\,\mu m$. (B) The time average of intensity for MinD (left) and MinE (right) in experiments (see Ref. [44] and [47]). The colors are scaled from 0 to 1. The main characteristics of high and low normalization are similar between A and B.

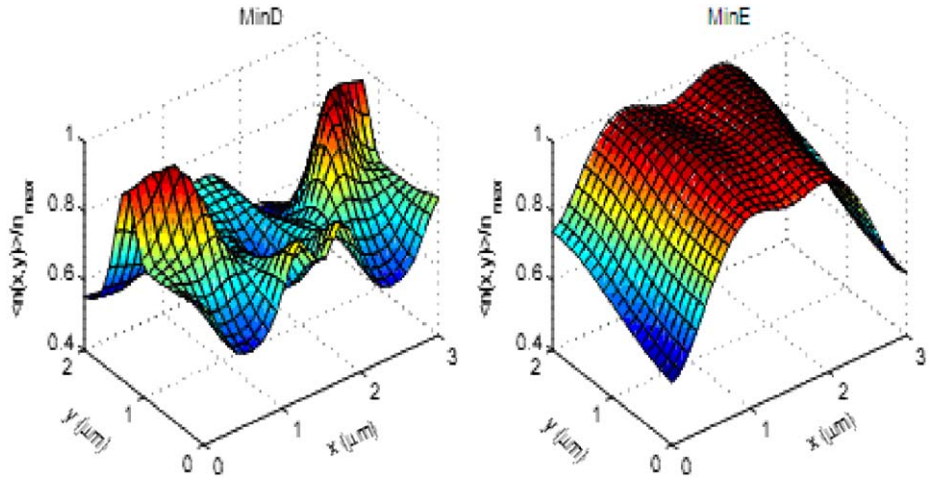

Fig. 8. The profiles of time averages MinD (left) and MinE (right) densities relative to their maxima, $n(x,y)/n_{max}$. The bacterial shape is $2 \times 3\,\mu m$.

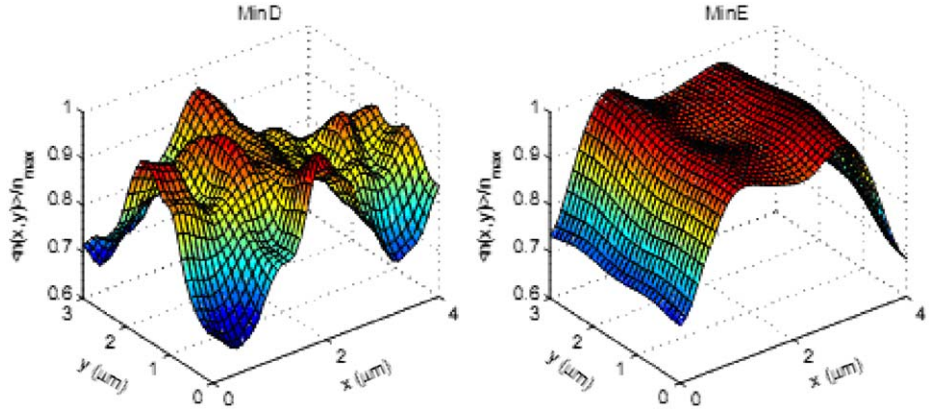

Fig. 9. The profiles of time averages MinD (left) and MinE (right) densities relative to their maxima, $n(x,y)/n_{max}$. The bacterial shape is $3 \times 4\,\mu m$.

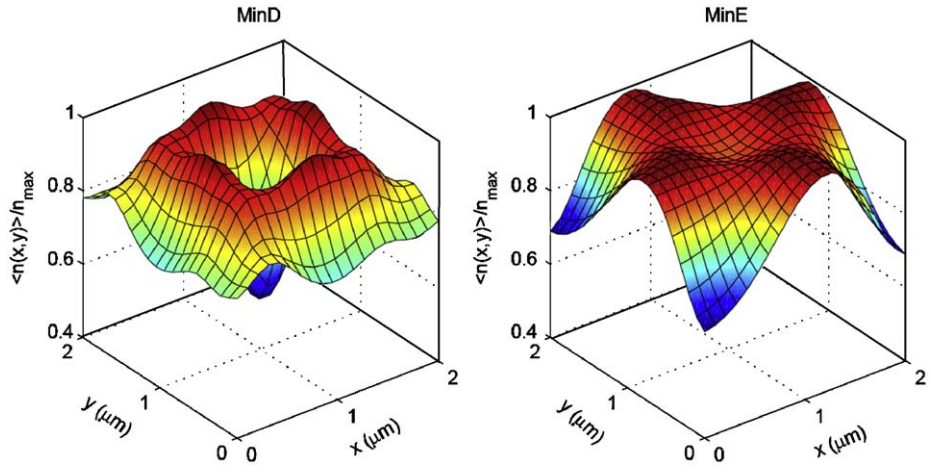

Fig. 10. The profiles of time averages MinD (left) and MinE (right) densities relative to their maxima, $n(x,y)/n_{max}$. The bacterial shape is $2 \times 2\,\mu m$.

the cell. Moreover, MinD and MinE in a square-shaped cell perform repeated lateral movements suggesting that these Min proteins do not assemble at the poles or ends of the axis (there being no obvious axis of the cell length) but can, in fact, assemble anywhere in the cell. This result suggests that protein oscillation governing cell division should not occur when an *E. coli* cell is square. Compared to those results by Huang and Wingreen [18], they also suggested that the Min protein comprises a general cell geometry detection mechanism that can dynamically reorganize division site placement in response to changes in cell shape.

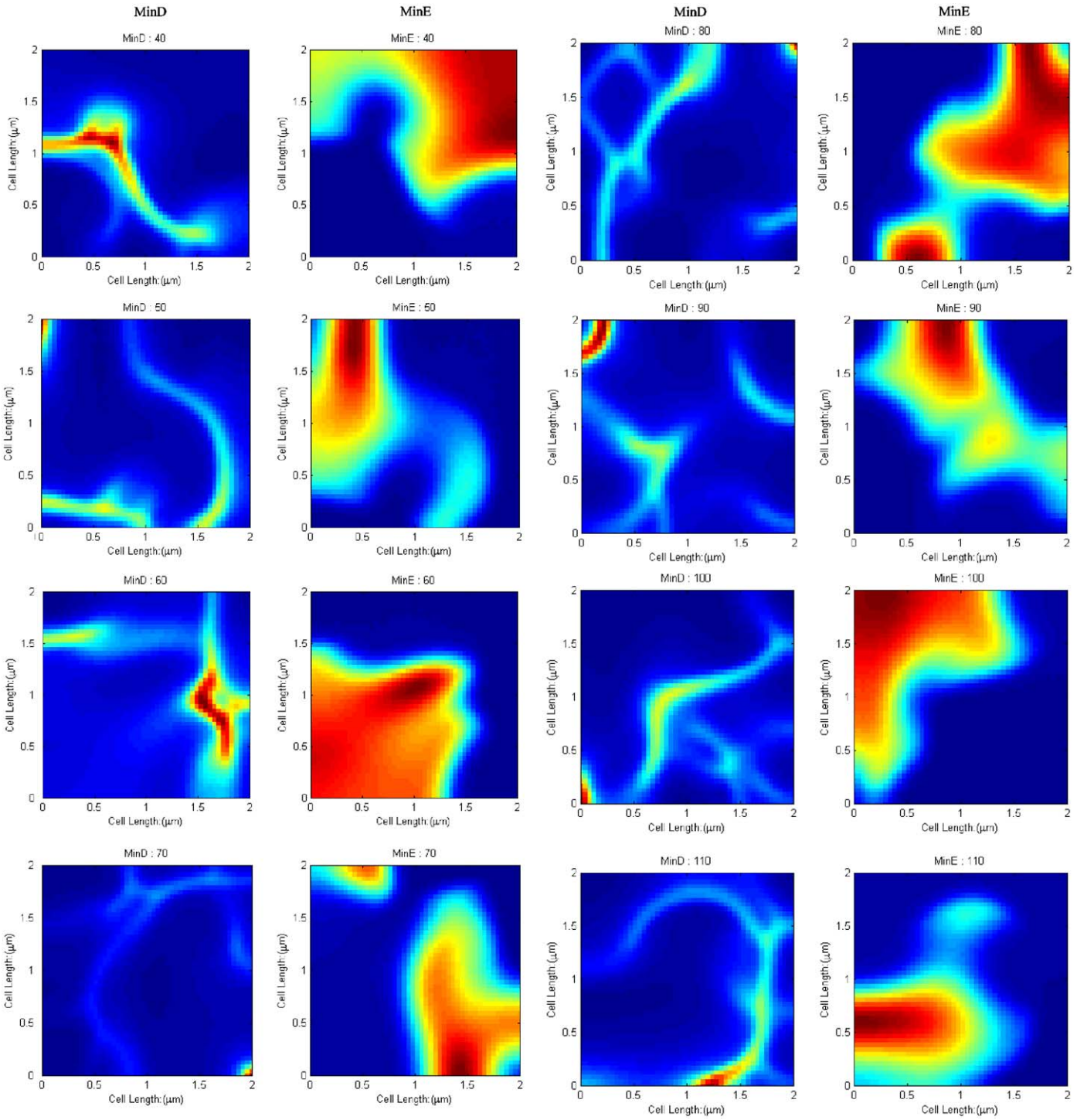

Fig. 11. The time series snapshots of dynamical patterns of MinD and MinE in 2×2 square shaped of bacteria. The dynamical patterns of MinD are seen in columns 1 and 3, while those of MinE are seen in columns 2 and 4. We monitored times range from 40 to 110 s.

Finally, we would like to mention that indeed *E. coli* are able to grow and divide as spheres and still generate two daughter cells of similar size. There are evidences from the recent study indicating that the Min system exerts spatial control of division site positioning in round cell (cocci) of *E. coli* [18,48]. Due to the fact that before the cell is divided, the Min system has to find the long axis. Hence the Min system in rod-shaped *E. coli* can find the obvious long axis so that the cell can divide into two daughter cells. For division in round cell, even there is no obvious long axis, cocci is still able to accurately divide along equatorial or alternating perpendicular planes into two daughter cells instead. In this process, the Min proteins oscillate to regulate a usual function of blocking polar division at the poles of the round cell. This consequently would allow the dividing plane around the equator to be consistently defined [49,50]. In square cell (as an approximate system of the real round cell) considered in our model, as a consequence of the dynamics used, the density of MinD and MinE in terms of time average cannot find the long axis (or dividing plane counterpart) so that MinD could not find the polar zones as well as

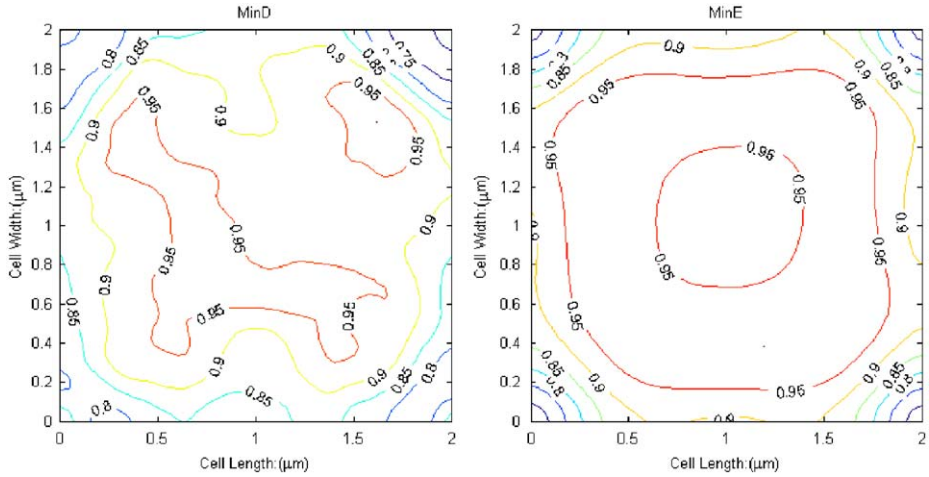

Fig. 12. Contour plots for MinD (left) and MinE (right) corresponding to the patterns given in Fig. 11.

MinE could not specify the midcell zone (Figs. 10 and 12). This could accordingly lead to malfunction in cell division. With this regards, one may consider the present model as a bit over-simplified model or the limitation of this LBM model in our case. As pointed out previously, the LBM is based on particle dynamics (mesoscale), its central contribution is thus the averaged macroscopic behavior leaving out the fluctuation. Hence one could (at least in principle) improve the model in two directions: complicating model by accounting more detailed mechanism especially using the experimental evidences or using microscopic scale model with fluctuation.

6. Concluding remarks and future works

Understanding of bacteria cell division is central for an understanding of microorganism as well as the origin of the life. This research has utilized the two-dimensional LBM to investigate the dynamic pole-to-pole oscillations of Min proteins, a mechanism used to determine the middle of a bacterial cell for division. We have developed a numerical scheme based on the LBM to simulate the coarse-grained coupled RDE model used to describe the MinD/MinE interaction in two dimensions. Good agreement between the experimental and numerical results is found, such as the time evolution of the MinD and MinE with the DIC monograph as observed in experiments. In addition, we have also investigated the possible evolutionary connection between cell shapes and cell division of *E. coli*. Interestingly, the limitation of LBM model and why our model fails to predict the cell division in the round cell have also been discussed.

The LBM approach provides a fast computational tool to study the deterministic models of protein oscillation. This finding suggests that the LBM is a useful scheme for simulating biological systems at the cellular level, especially those which are governed by the RDE. In a future work, we will generalize the current LBM so that it can be used to study the effects of in-homogeneity in the intracellular space and the possibility of an asymmetrical cell division. Since the LBM is a method based on kinetic theory, it should be a suitable alternative for studying the effects of various factors on cell division of a bacterium. Lastly with the main advantage of the LBM in which the particle interpretation allows the use of very simple boundary conditions so that the parallel implementation may be used even for very complex cell geometry. However, LBM neglect atomistic interaction and fluctuation effect.

Conflict of interest statement

None declared.

Acknowledgments

We would like to acknowledge several colleagues who contributed in different ways to this work. We also thank anonymous referees for such useful comments and suggestions to better this paper. The research funding is supported by The National Center for Genetic Engineering and Biotechnology (BIOTEC), The Thailand Research Fund (TRF), The Commission on Higher Education (CHE), The Thailand Center of Excellence in Physics (ThEP), the support of The Development and Promotion of Science and Technology Talent Project (DPST) and The Thailand's Software Industry Promotion Agency (Public Organization).

References

[1] C.L. Woldringh, E. Mulder, P.G. Huls, N. Vischer, Toporegulation of bacteria division according to the nucleiod occlusion model, Res. Microbiol. 142 (1991) 309–320.
[2] P.A.J. de Boer, R.E. Crossley, A division inhibitor and a topological the specificity factor coded for by the minicell locus determine proper placement of division septum in *E.coli*, Cell 56 (1989) 614–649.
[3] P.A.J. de Boer, R.E. Crossley, L.I. Rothfield, Central role for the *Escherichia coli* Min C gene product in two different cell division inhibition systems, Proc. Natl. Acad. Sci. USA 87 (1990) 1129–1133.
[4] P.A.J. de Boer, R.E. Crossley, A.R. Crossley, L.I. Rothfield, The Min protein is a membrane ATPase required for the correct placement of the *Escherichia coli* division site, Eur. Mol. Biol. Org. J. 10 (1991) 4371–4380.
[5] J. Huang, J.C. Cao, J. Lutkenhaus, Interaction between FtsZ and inhibitors of cell division, J. Bacteriol. 178 (1996) 5080–5085.
[6] Z. Hu, J. Lutkenhaus, Topological regulation of cell division in *E. coli* involves rapid pole to pole oscillation of the division inhibitor MinC under the control of MinD and MinE, Mol. Microbiol. 34 (1999) 82–90.
[7] D.M. Raskin, P.A.J. De Boer, Min DE-dependent pole to pole oscillation of division inhibitor MinC in *E. coli*, J. Bacteriol. 181 (1999) 6419–6424.
[8] X. Fu, Y.L. Shih, Y. Zhang, L.I. Rothfield, The MinE ring required for proper placement of the division site is a mobile structure that changes its cellular location during the *Escherichia coli* division cycle, Proc. Natl. Acad. Sci. USA 98 (2001) 980–985.
[9] D.M. Raskin, P.A.J. De Boer, Rapid pole-to-pole oscillation of a protein required for directing to the middle of *E. coli*, Proc. Natl. Acad. Sci. USA 96 (1999) 4971–4976.
[10] S.L. Rowland, X. Fu, M.A. Sayed, Y. Zhang, W.R. Cookand, L.I. Rothfield, Membrane redistribution of the *Escherichia coli* MinD protein induced by MinE, J. Bacteriol. 182 (1997) 613–619.
[11] K.C. Huang, Y. Meir, N.S. Wingreen, Dynamic structures in *E. coli*: spontaneous formation of MinE rings and MinD polar zones, Proc. Natl. Acad. Sci. USA 100 (2003) 12724–12728.

[12] D.M. Raskin, P.A.J. De Boer, The MinE ring: an FtsZ-independent cell structure required for selection of the correct division site in *E. coli*, Cell 91 (1997) 685–694.
[13] C.A. Hale, H. Meinhardt, P.A.J. De Boer, Dynamic localization cycle of the cell division regulator MinE in *E. coli*, Euro. Mol. Biol. Org. J. 20 (2001) 1563–1572.
[14] M. Howard, A.D. Rutenberg, S. De Vet, Dynamic compartmentalization of bacteria: accurate division in *E. coli*, Phys. Rev. Lett. 87 (2001) 278102 (1)–278102(4).
[15] H. Meinhardt, P.A.J. De Boer, Pattern formation in *Escherichia coli*: a model for the pole-to-pole oscillations of Min proteins and the localization of the division site, Proc. Natl. Acad. Sci. USA 98 (25) (2001) 14202–14207.
[16] K. Kruse, A dynamics model for determining the middle of *E. coli*, Biophys. J. 82 (2002) 618–627.
[17] M. Howard, A.D. Rutenberg, Pattern formation inside bacteria: fluctuation due to the low copy number of proteins, Phys. Rev. Lett. 90 (2003) 128102 (1)–128102(4).
[18] K.C. Huang, N.S. Wingreen, Min-protein oscillations in round bacteria, Phys. Biol. 1 (2004) 229–235.
[19] S. Chen, D.G. Doolen, Lattice Boltzmann method for fluid flows, Ann. Rev. Fluid Mech. 30 (1998) 329–364.
[20] N.S. Martys, H.D. Chen, Simulation of multicomponent fluids in complex three-dimensional geometries by the lattice Boltzmann method, Phys. Rev. E 53 (1996) 743–750.
[21] S. Chen, H. Chen, D. Martinez, W. Matthaeus, Lattice Boltzmann model for simulation of magnetohydrodynamics, Phys. Rev. Lett. 67 (1991) 3776–3779.
[22] D.O. Martinez, S. Chen, W.H. Matthaeus, Lattice Boltzmann magnetohydrodynamics, Phys. Plasmas 1 (1994) 1850–1867.
[23] M. Hirabayashi, Y. Chen, H. Ohashi, New lattice-Boltzmann model for magnetic fluids, Phys. Rev. Lett. 87 (2001) 178301(1)–178301(4).
[24] P. Dellar, Lattice kinetic schemes for magnetohydrodynamics, J. Comp. Phys. 179 (2002) 95–126.
[25] G.D. Doolen, Lattice Gas Methods: Theory, Applications and Hardware, second ed., MIT, Cambridge, MA, 1991.
[26] R.G.M. Vander Sman, M.H. Ernst, Advection–diffusion lattice Boltzmann scheme for irregular lattices, J. Comp. Phys. 60 (2000) 766–782.
[27] S.P. Dawson, S. Chen, G.D. Doolen, Lattice Boltzmann computations for reaction–diffusion equations, J. Chem. Phys. 98 (1993) 1514–1523.
[28] R. Blaak, P.M. Sloot, Lattice dependence of reaction–diffusion in lattice Boltzmann modeling, Comp. Phys. Commun. 129 (2000) 256–266.
[29] G. Yan, L. Yuan, Lattice Boltzmann simulation for the spiral waves in the excitable medium, Nonlinear Sci. Numer. Sim. 5 (2000) 147–150.
[30] Q. Li, C. Zheng, N. Wang, Spiral waves in CIMA model and its LBGK simulation, Nonlinear Sci. Numer. Sim. 6 (2001) 68–73.
[31] C. Migliorini, Y.H. Qian, H. Chen, E. Brown, R. Jain, L. Munn, Red blood cells augment leukocyte rolling in a virtual blood vessel, Biophys. J. 84 (2002) 1834–1841.
[32] C.H. Sun, C. Migliorini, L. Munn, Red blood cells initiate leukocyte Rollin in postcapillary expansions: a lattice Boltzmann analysis, Biophys. J. 85 (2003) 208–222.
[33] M. Hirabayshi, M. Ohta, D.A. Rufenacht, B. Chopard, A lattice Boltzmann study of blood flow in stinted aneurism, Futer. Gen. Comp. Sys. 20 (2004) 925–934.
[34] Y.H. Qian, D. Dhumieres, P.A. Lallemann, Lattice BGK models for Navier–Stokes equation, Europhys. Lett. 17 (1992) 479–484.
[35] H. Chen, S. Chen, W.H. Matthaeus, Recovery of the Navier–Stokes equations using a lattice-gas Boltzmann method, Phys. Rev. A 45 (1992) R5339–R5342.
[36] R. Benzi, S. Succi, M. Vergassola, The lattice Boltzmann equation: theory and applications, Phys. Rev. Rep. 222 (1992) 145–197.
[37] R. Mei, L.S. Luo, W. Shyy, An accurate curved boundary treatment in the lattice Boltzmann method, J. Comp. Phys. 155 (1999) 307–330.
[38] J.G. Zhou, Lattice Boltzmann Methods for Shallow Water Flows, Germany, 2004.
[39] X. He, L.S. Luo, A priori derivation of the lattice Boltzmann equation, Phys. Rev. E 55 (1997) R6333–R6336.
[40] X. He, L.S. Luo, Theory of the lattice Boltzmann method: from the Boltzmann equation to the lattice Boltzmann equation, Phys. Rev. E 56 (1997) 6811–6817.
[41] S. Chen, D.O. Martinez, R. Mei, On boundary conditions in lattice Boltzmann methods, Phys. Fluids 8 (1996) 2527–2536.
[42] Q. Zou, X. He, On pressure and velocity boundary conditions for the lattice Boltzmann BGK model, Phys. Fluids 9 (1997) 6202–6205.
[43] X. Zhang, J.W. Crawford, A.G. Bengough, I.M. Young, On boundary conditions in the lattice Boltzmann model for advection and anisotropic dispersion equation, Adv. Water Resour. 25 (2002) 601–609.
[44] U. Junthorn, S. Unai, P. Kanthang, W. Ngamsaad, C. Modchang, W. Triampo, C. Krittanai, D. Triampo, Y. Lenbury, Single-particle tracking method for quantitative tracking and biophysical study of MinE protein, J. Korean Phys. Soc. 52 (2008) 639–648.
[45] C.L. Woldringh, N.B. Grover, R.F. Rosenberger, A. Zaritsky, Dimensional rearrangement of rod-shaped bacteria following nutritional shift-up. II. Experiments with *Escherichia coli*, J. Theor. Biol. 86 (1980) 441–454.
[46] D. Bramhill, C.M. Thompson, GTP-dependent polymerization of *Escherichia coli* FtsZ protein to form tubules, Proc. Natl. Acad. Sci. USA 91 (1994) 5813–5817.
[47] S. Unai, P. Kanthang, U. Junthon, W. Ngamsaad, W. Triampo, C. Modchang, C. Kritanai, Quantitative analysis of time series fluorescence microscopy using single particle tracking method: application to MinD protein dynamics, Biologia 64 (1) (2009) 27–42.
[48] B.D. Corbin, X.C. Yu, W. Margolin, Exploring intracellular space: function of the Min proteins system in round-shaped *E. coli*, Eur. Mol. Biol. Org. J. 21 (2002) 1998–2008.
[49] J. Szeto, S. Ramirez-Arcos, C. Raymond, L.D. Hicks, C.M. Kay, J.A.R. Dillon, Gonococcal MinD affects cell division in *Neisseria gonorrhoeae* and *Escherichia coli* and exhibits a novel self-interaction, J. Bateriol. 183 (2001) 6253.
[50] S. Ramirez-Arcos, J. Szeto, J.A.R. Dillon, W. Margolin, Conservation of dynamic localization among MinD and MinE orthologues: oscillation of *Neisseria gonorrhoeae* proteins in *Escherichia coli*, Mol. Microbiol. 46 (2002) 493–504.

Somchai Sriyab was born in Lamphoon, Thailand, in 1978. He received an M.Sc. degree in Applied Mathematics from Mathematics Department, Mahidol University, Bangkok, Thailand, in 2004. Now he is a Ph.D. candidate in Mathematics department, in the same university. His research interests focus on mathematical biology and LBM.

Jiraporn Yojina was born in Lumphoon, Thailand, in 1978. She received an M.Sc. degree in Applied Mathematics from Mathematics Department, Mahidol University, Bangkok, Thailand, in 2004. Now she is a Ph.D. candidate in Mathematics department, in the same university. Her research interests focus on mathematical biology and medicine.

Waipot Ngamsaad was born in Uttaraditr, Thailand, in 1980. He received an M.Sc. degree from Physics Department, Mahidol University, Bangkok, Thailand, in 2005. Now he is a Ph.D. candidate in Physics Department, in the same university. His research interests focus on computational biophysics and LBM.

Pisan Kangthang was born in Bangkok, Thailand, in 1980. He received an M.Sc. degree from Physics Department, Mahidol University, Bangkok, Thailand, in 2003. Now he is a Ph.D. candidate in Physics Department, in the same University. His research interests focus on biophysics and simulations.

Charin Modchang was born in Pichit, Thailand, in 1983. He received a B.Sc. degree from Physics Department, Mahidol University, Bangkok, Thailand, in 2005. Now he is a Ph.D. candidate in Physics Department, in the same University. His research interests focus on computational biophysics and theoretical biology and medicine.

Narin Nuttavut was born in Nakhonprathom Province, Thailand, in 1972. He received a Ph.D. in Physics from Imperial College London, UK, in 2001. After graduation, he has been with Mahidol University, Thailand, where he is an Assistant Professor in Physics. His research interests focus on biophysics and modeling.

Yongwimon Lenbury was born in Bangkok, Thailand, in 1952. She received a Ph.D. in Mathematics from Vanderbilt University. After graduation, she has been with Mahidol University, Thailand, where she is a Professor in Mathematics. Her research interests focus on applied mathematics and modeling.

Chartchai Krittanai was born in Nakhonprathom Province, Thailand, in 1969. He received a Ph.D. in Biochemistry and Biophysics from Oregon State University, USA, in 1997. After graduation, he has been with Mahidol University, Thailand, where he is now an Associate Professor in biophysics and molecular biology. His research interests focus on biochemistry and biophysics.

Wannapong Triampo was born in Nakhonratchasima Province, Thailand, in 1970. He received a Ph.D. in Physics from Virginia Tech, USA, in 2001. After graduation, he has been with Mahidol University, Thailand, where he is an Assistant Professor in Physics. His research interests focus on biophysics and modeling.